STANFORD LINEAR ACCELERATOR CENTER

SLD Experiment
At the SLAC Linear Collider

USA – Boston, Colorado, Colorado State, Johns Hopkins, Lawrence Berkeley Lab, U Mass, MIT, Mississippi, Oregon, Rutgers,Tennessee, UC Santa Barbara, UC Santa Cruz, SLAC, Vanderbilt, Washington, Wisconsin, Yale
Italy – Frascati, Perugia
Japan – Aomori, Nagoya, Tohoku
Russia – Moscow State
Korea – Sogang, Soongsil
UK – Oxford, Rutherford Appleton Lab

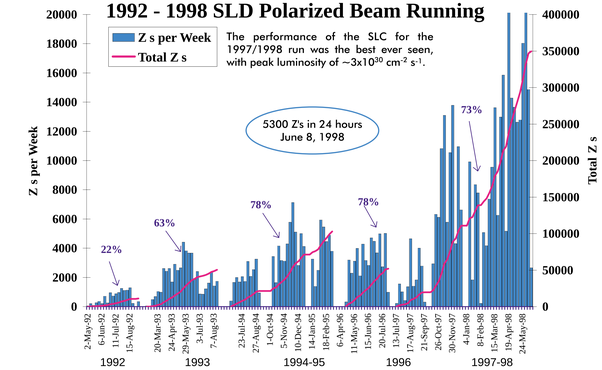

Vertex Detector

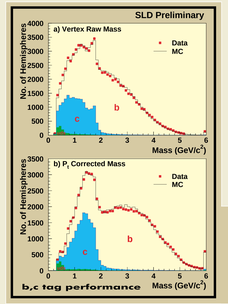

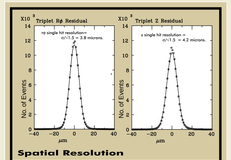

Spatial resolution measured from tracks with hits on each of the 3 layers.

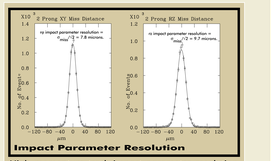

High momentum track impact parameter resolution measured from 2-prong miss distances of mu-pair events. The multiple scattering contribution to impact parameter resolution is approximately 35μm/Psin^3/2θ for both rφ and rz views (P in GeV/c).

tag	efficiency	purity
b hemisphere	54%	98%
c hemisphere	21%	73%
c event tag	41%	86%

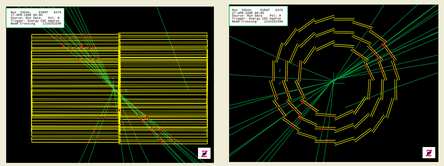

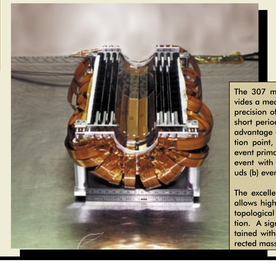

The 307 megapixel CCD vertex detector provides a measurement of the primary vertex to a precision of 3.5 μm in x,y by averaging over a short period of hadronic Z^0 events. This takes advantage of the small and stable SLC interaction point, 2x1x700 μm³ (σ_x x σ_y x σ_z). The event primary vertex Z is reconstructed event by event with a resolution of 9 (17) microns for uds (b) events.

The excellent resolution of the vertex detector allows high performance b,c-tags through 3-D topological vertex and vertex mass reconstruction. A significant tagging enhancement is obtained with a kinematic correction (see P_t corrected mass figure) for missing neutrals.

B Mixing

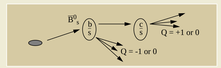

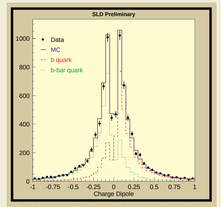

The Charge Dipole technique exploits the B → D cascade charge structure by reconstructing both secondary and tertiary decay vertices. B and $\bar{B}$ decays are then separated based on the sign of the charge difference between the secondary and tertiary vertices. In the case of B_s decays, ~79% are correctly signed.

Heavy Flavors

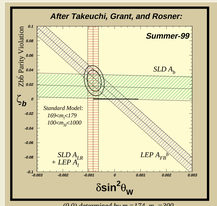

(0,0) determined by m_t=174, m_H=300, α_s=0.119 α_{EM}=1/128.905

The Zbb̄ vertex global fit following the scheme of Takeuchi et al. The Standard Model is defined at (0,0) with variations of m_t and m_H spanning the horizontal line. The fit result 68% and 90% CL contours are plotted as ellipses.

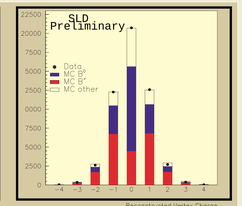

Separation between B^+ and B^0 decays is achieved by reconstructing the total charge of topological secondary vertices, allowing the world's best measurements of individual B hadron lifetimes (see table).

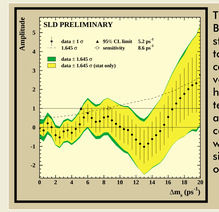

The time dependence of B_s-$\bar{B}_s$ mixing has been studied using semileptonic and inclusive decays. The high-resolution vertex detector allows highly efficient topological techniques to be used and provides excellent decay length resolution which is crucial to be sensitive to the very fast B_s oscillations.

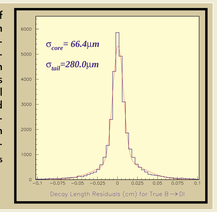

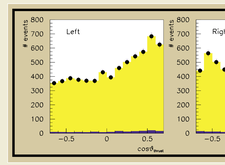

The polarized electron beam provides high sensitivity measurements of A_f, the parity violation parameter in the final state Zff coupling. An example of raw asymmetries for left- and right-handed beams is shown for an A_b measurement using K^{+-} identified by the CRID (exploiting the b→c→s decay signature for signing the b-quark direction in tagged b events). The results of a number of complementary measurements of A_b and of similar measurements of A_c, A_s, $A_τ$, $A_μ$, and A_e are summarized in the table.

Cherenkov Ring Imaging Particle ID

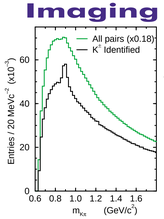

Distributions of the $K^+\pi^-$ (left) and K^+K^- (right) invariant mass for all pairs of oppositely charged tracks (green histograms) and those in which the kaons are identified in the CRID (black histograms). Signatures for $K^{*0}(892)\rightarrow K^+\pi^-$ and $\phi\rightarrow K^+K^-$ are clear (almost invisible) with (without) kaon identification.

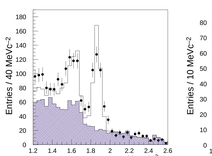

Distributions (dots) of the a) $K^-\pi^+$ and b) $K^+K^-\pi^+$ invariant mass for sets of tracks that form a secondary vertex and in which the kaons are identified in the CRID. The predictions of the simulation for the total (histogram) and background (hatched histogram) distributions are also shown. A clear signal for $D^0\rightarrow K^-\pi^+$ is visible in (a), as is the satellite peak from $D^0\rightarrow K^-\pi^+\pi^0$. A signal for $D_s^+\rightarrow K^+K^-\pi^+$ is visible in (b).

Electroweak

Since 1992, improvements of the polarized electron source and of spin transport in the SLC have led to 75% peak polarization, measured by the Compton polarimeter.

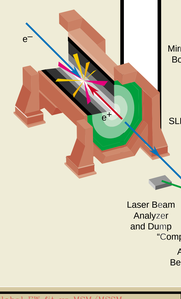

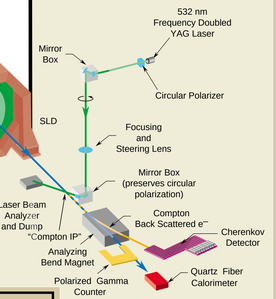

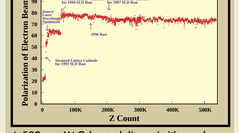

A 532 nm YAG laser delivers (with randomly switched helicity) 99.9% circularly polarized photon pulses at about 17 Hz, into head-on (10 mrad angle) collision with the outgoing electron beam. The polarimeter spectrometer includes a transversely segmented 9-channel Cherenkov counter that is sensitive to Compton scattered electrons. Two detectors positioned along the neutral beamlines are sensitive to Compton scattered photons (a single-channel Cherenkov counter and a quartz fiber calorimeter), and with the positron beam disabled provide better than 0.5% cross-check of the main Cherenkov polarimeter calibration. The system achieves a systematically limited relative precision of about 0.5%.

Preliminary Results

$\tau(B^+) = 1.623 \pm 0.020$ (stat) ± 0.034 (syst) ps
$\tau(B^0) = 1.589 \pm 0.021$ (stat) ± 0.043 (syst) ps
$\tau(B^+)/\tau(B^0) = 1.037 -0.024+0.025$ (stat) ± 0.024 (syst)
$\Delta m_s = 0.531 \pm 0.043$ (stat) ± 0.034 (syst) ps^{-1}
$\Delta m_s < 5.2\ ps^{-1}$ and $11.3 < \Delta m_s < 14.2\ ps^{-1}$ excluded at 95% C.L.
$R_b = 0.2159 \pm 0.0014$ (stat) ± 0.0014 (syst)
$R_c = 0.169 \pm 0.005$ (stat) ± 0.004 (syst)
$A_b = 0.905 \pm 0.017$ (stat) ± 0.020 (syst)
$A_c = 0.634 \pm 0.021$ (stat) ± 0.017 (syst)
$A_s = 0.85 \pm 0.06$ (stat) ± 0.07 (syst)
$A_τ = 0.142 \pm 0.016$ (stat) ± 0.004 (syst)
$A_μ = 0.137 \pm 0.016$ (stat) ± 0.001 (syst)
$A_e = 0.1558 \pm 0.0060$ (stat) ± 0.0022 (syst)

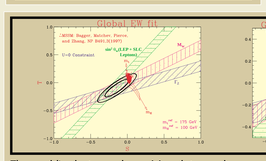

The world's electroweak precision data can be compared in the context of a general class of models using the S,T,U scheme of Peskin and Takeuchi. The Standard Model (SM) and related models, including supersymmetric (SS) models, are included in this general class, a key feature of which is that radiative corrections are dominated by effects on the gauge boson propagators. The T parameter is a measure of weak isospin-violating loop effects (such as those due to the heavy top quark), while the S parameter measures the generally smaller weak isospin-conserving corrections.

The three most precise measurements presently available – the Z width, W mass, and $\sin^2\theta_{eff}$ – are shown as bands in the ST plane. The fit ellipse (68% and 95% CL contours) to the complete set of electroweak data (from LEP/SLC, FNAL Tevatron, ν-DIS, and atomic parity violation) is also given. The allowed SM region, given the present precision top mass from FNAL and the direct search limits on the SM Higgs from LEP, is the banana-shaped region. Also shown is the region of ST space covered by the minimal SS model (MSSM). The SLD and LEP lepton-based mixing angle results, and the new measurements of W mass favor a lighter Higgs -- which is also the region preferred by the MSSM.

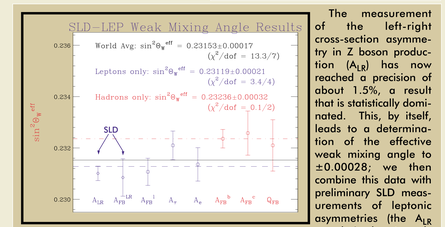

The measurement of the left-right cross-section asymmetry in Z boson production (A_{LR}) has now reached a precision of about 1.5%, a result that is statistically dominated. This, by itself, leads to a determination of the effective weak mixing angle to ±0.00028; we then combine this data with preliminary SLD measurements of leptonic asymmetries (the A_{LR} sample is almost purely hadronic Z decays), to obtain a precision of ±0.00026. The SLD A_{LR} result is more precise, with substantially smaller systematic errors, than any other method. The different Z pole determinations are shown above. Presently, the SLD and LEP lepton-based result differs from the LEP bottom and charm hadron-based average by about 3.1 standard deviations.

QCD

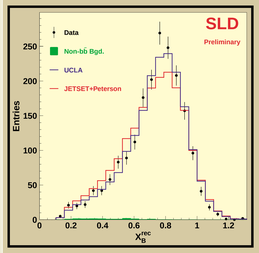

Uncorrected distribution (dots) of scaled B-hadron energies measured using a novel, inclusive, kinematic technique based on charged tracks only. The unprecedented precision and coverage, over the full kinematic range from the B-hadron mass to the beam energy, allow stringent tests of predicted forms for this distribution. For example, the prediction of the UCLA fragmentation model (blue histogram) is consistent with the data, whereas that of the Peterson model (with a fitted parameter ε_b=0.006) within the JETSET generator (red histogram) is not. Several other models and ad hoc functional forms are also excluded. Using a set of eight shapes consistent with the data, we measure a value of $\langle x_B \rangle = 0.714 \pm 0.005(\text{stat.}) \pm 0.007(\text{syst.}) \pm 0.002$ (model) (Preliminary); the uncertainty from model dependence is small.

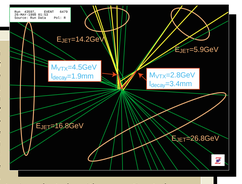

Event display of the region within 0.5 cm of the interaction point (IP) for a candidate $e^+e^-\rightarrow q\bar{q}g\rightarrow q\bar{q}b\bar{b}$ event, showing extrapolated charged tracks with vertex hits. A high-mass secondary vertex is found in each of the two jets with the smallest angle between them. The tracks shown in yellow are assigned to a vertex and the displacements from the IP are indicated by the red lines. A sample of 62 candidate events is selected, with an estimated background of 27.6 ± 1.2 events, corresponding to a probability for a hadronic Z^0 decay to contain a g→bb splitting of g_{bb} = 0.00307 ± 0.00071 (stat.) ± 0.00066 (syst.) (Preliminary).

Uncorrected distributions of the absolute difference in rapidity, y, for identified p-p̄ (black histogram) and p-p/p̄-p̄ (green histogram) pairs in hadronic Z^0 decays. The p-p̄ excess at low |Δy| indicates local conservation of baryon number. Similar short-range correlations are observed for all pair combinatons of $\pi^\pm$, $K^\pm$ and p/p̄, indicating local strangeness and isospin conservation, and also local charge sharing between mesons and baryons and between strange and nonstrange particles. b) The subset of (a) for which both particles have p>9 GeV/c. A long-range correlation is now also evident, due to events with a leading baryon in the q jet and a leading antibaryon in the q̄ jet. Long-range correlations are observed for all pair combinatons, providing new information on leading particle production. c) Distribution of the difference between the signed rapidities for an identified p and p̄, where y>0 (y<0) for tracks in the (anti)quark hemisphere. The shift in the central peak toward positive values is a direct indication of baryon number ordering along the qq̄ axis. This effect is present at all momenta (see (d)), indicating that this is a fundamental property of jet fragmentation, and not simply a leading particle effect.

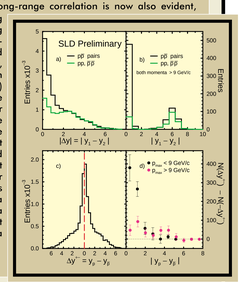

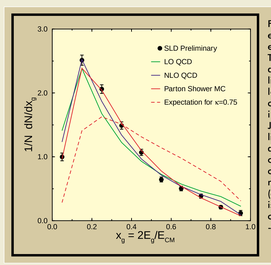

First measurement (dots) of the gluon energy distribution in 3-jet $e^+e^-\rightarrow b\bar{b}g$ events over the full kinematic range. The predictions of leading (green line) and next-to-leading order QCD (blue line) are inconsistent with the data at low energy, where higher order contributions are expected to be important. The prediction of the JETSET parton shower simulation (red line) is consistent with the data. This distribution is sensitive to the presence of an anomalous chromomagnetic coupling at the $b\bar{b}g$ vertex, with a relative coupling parameter κ (dashed red line). Our fitted value of κ is consistent with zero, and we calculate 95% C.L. limits of $-0.11 < \kappa < 0.08$.